

Quantitative implementation of Preisach-Mayergoyz space to find static and dynamic elastic moduli in rock

R. A. Guyer,¹ K. R. McCall,² G. N. Boitnott,³
L. B. Hilbert Jr.,^{4,5} and T. J. Plona⁶

Abstract. In this paper we describe the analysis of quasi-static stress-strain data using a Preisach-Mayergoyz (PM) [after *Preisach*, 1935; *Mayergoyz*, 1985] space picture for the elastic behavior of rock. In contrast to the traditional analytic approach to stress strain (an energy density as a function of the strain invariants), the PM space picture reproduces hysteresis and discrete memory seen in the data. In addition, the PM space picture establishes a relationship between experimental data and a number density ρ of microscopic mechanical units within the rock. The density ρ allows us to make quantitative predictions of dynamic elastic properties. Determining ρ from quasi-static stress-strain data requires us to solve a highly underdetermined inverse problem. We explore the following three methods of solving the inverse problem: simulated annealing, normal modes, and exponential decay. All three methods are tested on a Berea sandstone data set and found to give an excellent description of stress versus strain. Choosing one method, the normal mode method, we analyze quasi-static stress-strain curves on two additional sandstones, namely, another sample of Berea and a sample of Castlegate sandstone. From the density ρ for each sample we predict the dynamic modulus as a function of pressure and the nonlinear elastic constants. For each of these cases the agreement between the predictions based on ρ and experiment is quite good. We establish that PM space provides a quantitative description of the elastic response of a rock and that PM space may be found by a variety of inversion methods.

Introduction

This paper is the second in a series on the elastic properties of rocks. In the first paper [*McCall and Guyer*, 1994] we introduced a description of rock elasticity that accounts for observed history and memory features. The central construct in the description was the Preisach-Mayergoyz (PM) space [after *Preisach*, 1935; *Mayergoyz*, 1985] in which the macroscopic material response is tracked using the density ρ of microscopic mechanical units (the density in PM space). *McCall and Guyer* [1994] showed that from ρ one could learn the elastic properties of the rock (the quasi-static modulus, the dynamic modulus, the strength of the cubic and quartic nonlinearities, etc.). In addition, we

suggested that quasi-static stress-strain measurements make it possible to learn ρ . Thus the recipe for the elastic properties of a rock is (1) collect quasi-static stress-strain data, (2) invert for ρ (PM space), and (3) predict elastic properties. The purpose of this paper is to demonstrate the determination of ρ from quasi-static stress-strain data. We call this the inverse problem. We use data on three sandstone samples called B1, B2, and C. We use the ρ that we find for these samples to determine their linear and nonlinear elastic properties.

We begin with a section reviewing the traditional theory of elastic wave propagation in nonlinear materials. Then we review the principal results of application of the PM space picture. Particular attention is given to the results leading to formulation of the inverse problem. Three methods for solving the inverse problem are described and applied to quasi-static stress-strain data on the B1 sample. We choose one of these methods, the method of normal modes, and apply it to all three data sets. We find ρ for each data set and show how ρ is used to predict the behavior of quasi-static stress-strain curves, predict the dynamic modulus, and predict the linear and nonlinear elastic coefficients.

Review of the Traditional Theory

The traditional theory of elastic wave propagation in a nonlinear material is based on expressing the energy density as a function of the scalar invariants of

¹Department of Physics and Astronomy, University of Massachusetts, Amherst.

²Department of Physics, University of Nevada, Reno.

³New England Research Incorporated, White River Junction, Vermont.

⁴Department of Materials Science and Mineral Engineering, University of California, Berkeley.

⁵Now at Failure Analysis Associates, Menlo Park, California.

⁶Schlumberger-Doll Research, Ridgefield, Connecticut.

Copyright 1997 by the American Geophysical Union.

Paper number 96JB03740.

0148-0227/97/96JB-03740\$09.00

the strain tensor. *Landau and Lifshitz* [1959] and *Murnaghan* [1951] find the equation of motion for the displacement field \mathbf{u} from

$$\mathcal{E} = \mu \epsilon_{ik}^2 + \left(\frac{K}{2} - \frac{\mu}{3} \right) \epsilon_{ii}^2 + \frac{A}{3} \epsilon_{ik} \epsilon_{il} \epsilon_{kl} + B \epsilon_{ik}^2 \epsilon_{il} + \frac{C}{3} \epsilon_{ii}^3 + \mathcal{O}(\epsilon^4), \quad (1)$$

$$\sigma_{ik} = \frac{\partial \mathcal{E}}{\partial (\partial u_i / \partial x_k)}, \quad (2)$$

$$\rho_0 \frac{\partial^2 u_i}{\partial t^2} = \frac{\partial \sigma_{ik}}{\partial x_k}, \quad (3)$$

where \mathcal{E} is the energy density, ρ_0 is a constant mass density, σ is the stress tensor, ϵ is the strain tensor,

$$\epsilon_{ik} = \frac{1}{2} \left(\frac{\partial u_i}{\partial x_k} + \frac{\partial u_k}{\partial x_i} + \frac{\partial u_l}{\partial x_i} \frac{\partial u_l}{\partial x_k} \right), \quad (4)$$

and $\mathcal{O}(\epsilon^4)$ represents terms of order ϵ^4 . The constants μ , K , A , B , and C are determined by experiment; for example, K is the bulk modulus of the material [*Winkler and Xingzhou*, 1996]. This formulation, in which the stress is taken to be an analytic function of the strain, has been very successful in describing the statics and dynamics of a wide variety of materials [*Ashcroft and Mermin*, 1976] including liquids [*Hamilton*, 1986].

Some of the best known properties of rocks are not described by the model embodied in these equations. For example, the dynamic modulus is usually greater than the static modulus [*Plona and Cook*, 1995], a result that was explained by appealing to a frequency effect or the difference between adiabatic (dynamic) and isothermal (static) measurements [*Biot*, 1956]. Also, the traditional theory provides neither a qualitative nor a quantitative explanation of a stress-strain equation of state with hysteresis and discrete memory [*Holcomb*, 1981]. In rock the stress is not an analytic function of the strain.

Review of the PM Space Picture

The elastic properties of a rock are due to the stress-strain response of many complex structural features such as cracks, joints, contacts, and grain boundaries. The behavior of any one of these structural features is complicated and often hysteretic. The experiments examined here, uniaxial stress strain over a fairly modest pressure range, are sensitive to the ensemble behavior of a vast number of structural features (10^9 – 10^{12} /cm³) in the rock. Thus we assign to each structural feature only those properties essential to assessing its participation in a uniaxial stress experiment. The structural features are replaced by simple mechanical units, springs that (1) enforce one of two displacements between their ends, l_o (o = open) at low pressure and l_c (c = closed) at high pressure and (2) respond hysteretically to the pressure they are called upon to support.

The mechanical units are hysteretic and respond to different opening and closing pressures. Thus the elastic

response of the units and the system as a whole depends on the pressure history of the rock. To describe the elastic behavior of a rock, we must know the pressure history and be able to relate the pressure history to the ensemble behavior of hysteretic mechanical units.

PM space is a construct that allows us to predict the ensemble behavior of many hysteretic mechanical units. PM space is a space in which the behavior of the mechanical units in the rock is tracked [*McCall and Guyer*, 1994]. In the following we review the contents and consequences of PM space (the forward calculation) and the construction of PM space from experimental data (the inverse calculation).

Forward Calculation

1. A mechanical unit that closes at pressure P_c and opens at pressure P_o is located in PM space at (P_c, P_o) . A mechanical unit that is open (closed) is said to be in state 0 (1). In the continuum limit, i.e., 10^9 – 10^{12} units/cm³, we employ the density $\rho(P_c, P_o) dP_c dP_o$, a measure of the fraction of mechanical units in $dP_c dP_o$ at (P_c, P_o) . A coarse-grained picture of PM space uses bins of area $\Delta P \times \Delta P$ at $(m\Delta P, n\Delta P)$, where $m, n = 0, \dots, N-1$. The minimum pressure is zero, and the maximum pressure is $P_{\max} = N\Delta P$. Thus the fraction of mechanical units in bin (m, n) is

$$\rho(m, n) = \int_{m\Delta P}^{(m+1)\Delta P} dP_c \int_{n\Delta P}^{(n+1)\Delta P} dP_o \rho(P_c, P_o). \quad (5)$$

All of the units in a bin are in the same state, 0 or 1; we write $\sigma_{mn} = 0, 1$.

2. A pressure protocol leads to a trajectory $E[\bar{P}_1, \dots, \bar{P}_L]$ that separates the region of PM space having units in state 1 from the region having units in state 0. The pressure extrema $\bar{P}_1, \dots, \bar{P}_L$ characterize the pressure protocol. In the coarse-grained picture the pressure protocol is coarse grained on scale ΔP .

3. The stress-strain relationship is

$$\epsilon = \Delta \epsilon f(E), \quad (6)$$

where $\Delta \epsilon = (l_o - l_c)/l_o$ and $f(E)$ is the fraction of mechanical units in state 1, i.e., the fraction of the mechanical units inside E . In the coarse grained picture

$$\epsilon = \Delta \epsilon \sum_{m=0}^{N-1} \sum_{n=0}^m \rho(m, n) \sigma_{mn}. \quad (7)$$

4. The static modulus measured with a pressure protocol cycling from zero to the maximum pressure and back to zero ($P = 0 \rightarrow N\Delta P \rightarrow 0$) has two values at each pressure. When the applied pressure is increasing,

$$K_{\uparrow}(P)^{-1} = \Delta \epsilon \int_0^P \rho(P, P_o) dP_o \quad (8a)$$

or

$$K_{\uparrow}(m)^{-1} = \Delta \epsilon \sum_{n=0}^m \rho(m, n) \Delta P. \quad (8b)$$

When the applied pressure is decreasing,

$$K_{\downarrow}(P)^{-1} = \Delta \epsilon \int_P^{P_{\max}} \rho(P_c, P) dP_c \quad (9a)$$

or

$$K_{\downarrow}(n)^{-1} = \Delta\epsilon \sum_{m=n}^{N-1} \rho(m, n) \Delta P. \quad (9b)$$

5. The dynamic modulus, i.e., the modulus appropriate to a small pressure oscillation, is given by

$$K_d^{-1}(P) = \Delta\epsilon A(P), \quad (10a)$$

where $A(P)$ is the diagonal part of ρ . In the coarse-grained picture

$$K_d^{-1}(m) = \Delta\epsilon \rho(m, m) \Delta P. \quad (10b)$$

6. The nonlinear elastic constants of traditional wave propagation theory may be calculated from the dynamic modulus. This calculation is described in the results section.

Inverse Calculation

Equations (5)–(10b) describe the results of forward modeling with PM space; that is, these equations show how to use the density in PM space to learn about the stress-strain relationship, the elastic moduli, etc. This forward modeling is illustrated in detail by *McCall and Guyer* [1994]. Equations (5)–(10b) also can be used in conjunction with experiment to learn the content of PM space, the density $\rho(P_c, P_o)$. A brief sketch of the inverse calculation, from experiment to PM space, is given by *Guyer et al.* [1995]. The development and use of this idea are the principal focus of this paper.

From (8b) we see that in the coarse-grained picture the inverse modulus, calculated from the stress-strain curve as the pressure is increased, is a column sum in PM space. That is, $K_{\uparrow}(m)$ is proportional to the fraction of mechanical units in bins $(m, 0) - (m, m)$ in PM space. (The absolute number of mechanical units in the bins is unimportant because the physical quantities of interest are related to the fractional content of the bins.) From (9b) we see that $K_{\downarrow}(n)$ is related to the row sum, the fraction of mechanical units in bins $(n, n) - (n, N - 1)$.

For a typical coarse graining of a stress-strain curve there are many more bins covering PM space than there are values of K_{\downarrow} and K_{\uparrow} , i.e., column and row constraints. For example, if $0 < P < 15$ MPa and $\Delta P = 0.5$ MPa, then the number of bins is $N(N + 1)/2 = 465$ and the number of constraints is $N + N = 60$. We want to invert known values of K_{\uparrow} and K_{\downarrow} to find $\rho(m, n)$. This problem is severely underdetermined (in the example above we have 465 unknowns and 60 equations); however, we can find a plausible solution using a variety of methods. We describe three methods we have used to address the problem of turning a stress-strain data set into ρ . We do this using three different data sets, B1, B2, and C. Each method has been used on all of the data sets. Here we show the use of each on the B1 data set. Then we choose one of the methods and use it to analyze the other two data sets.

One of our aims is to show that the inversion of stress-strain data is feasible and useful. Ultimately, we want

an optimum data set and computational strategy for uncovering the elastic features of interest. We expect this to involve a flexible and precise experimental setup working interactively with a flexible and facile computational apparatus.

Methods of Inversion

We illustrate three methods of inverting stress-strain curves to find $\rho(m, n)$. The problem is severely underdetermined; thus the solution is not unique. The three methods of inversion are simulated annealing (SA), normal mode analysis (NM), and exponential decay (ED). The data we use for the inversions are always a subset of the data available. We use the inversion results to predict additional parts of the data sets to establish predictive capability.

Simulated Annealing

The equations for $K_{\uparrow}^{-1}(i)$ and $K_{\downarrow}^{-1}(i)$, $i = 0, \dots, N - 1$, are a set of constraints C_k , $k = 0, \dots, 2N - 1$, on the $N(N + 1)/2$ numbers $\rho(m, n)$, $m = 0, \dots, N - 1$, $n = 0, \dots, m$. The constraints can be used to determine a PM space energy to be minimized,

$$E_C = \frac{1}{2} \sum_{k=0}^{2N-1} (C_k - S_k[\rho])^2, \quad (11)$$

where

$$S_j = \sum_{n=0}^j \rho(j, n), \quad (12a)$$

$$S_{N+j} = \sum_{m=j}^{N-1} \rho(m, j), \quad (12b)$$

and $j = 0, \dots, N - 1$. Variation of the energy E_C with respect to $\rho(m, n)$ leads to (8b)–(9b). To these modulus constraints we add the requirement of smoothness in the form of an energy that depends on the gradient of ρ (springs in the x and y directions), for example,

$$E_S = \frac{1}{2} \sum_{m=0}^{N-2} \sum_{n=0}^m [\rho(m+1, n) - \rho(m, n)]^2 + \frac{1}{2} \sum_{m=1}^{N-1} \sum_{n=0}^{m-1} [\rho(m, n+1) - \rho(m, n)]^2. \quad (13)$$

The total energy of PM space is $E = E_C + \lambda E_S$, where λ is a parameter set to maximize smoothness without compromising the primary constraints embodied in E_C . We minimize E computationally, using the following algorithm.

1. Load the bins in PM space at random with N_0 mechanical units. Because we want the fraction of units $f(E)$ in state 1 (see (6)), we are free to choose N_0 for convenience, e.g., $N_0 = 5000$. Denote the arrangement of mechanical units χ_0 .

2. Calculate the energy $E[\chi_0] = E_C[\chi_0] + \lambda E_S[\chi_0]$ of this initial configuration of the mechanical units.

3. Make a rearrangement of the mechanical units by choosing the address of two bins at random and moving one mechanical unit from the first bin to the second bin.

4. Calculate the energy $E[\chi_1] = E_C[\chi_1] + \lambda E_S[\chi_1]$ of the new configuration of the mechanical units. If $E[\chi_1] < E[\chi_0]$, accept the configuration χ_1 . If $E[\chi_1] > E[\chi_0]$, accept the configuration with probability $p = \exp[-(E[\chi_1] - E[\chi_0])/kT]$, where kT is a control parameter, the analog of temperature in a thermodynamic system. This acceptance scheme is called the Metropolis algorithm [Metropolis *et al.*, 1953].

5. Return to item 3, gradually lowering the value of the control parameter kT .

This procedure is stopped when the energy has been minimized or when it leads to no important further evolution in the energy. A more complete description of simulated annealing methods is given by Press *et al.* [1992]. Simulated annealing has the advantage of permitting evolution among configurations in a manner analogous to the evolution of a physical system at finite temperature; the system attempts to reach the lowest-energy state by a multiplicity of routes that are not available at absolute zero.

The degree to which the total energy E respects the smoothness constraint depends upon the value of λ . If λ is very large, the SA procedure generates a smooth solution that only weakly satisfies the modulus constraints. In the opposite limit, $\lambda = 0$, the solution satisfies the modulus constraints exactly and is one of a large number of degenerate, nonsmooth solutions.

Guyer *et al.* [1995] used a SA procedure to invert a data set on Berea sandstone to determine $\rho(m, n)$. Among the qualitative results was that the density in PM space is composed of two parts, a diagonal or non-hysteretic part containing a majority fraction of the mechanical units and an off-diagonal, background, or hysteretic part. That is

$$\rho(m, n) = A(m)\delta_{m,n} + \rho_B(m, n), \quad (14)$$

where $A(m)$ is the nonhysteretic part of $\rho(m, n)$ and $\rho_B(m, n)$ is the background or hysteretic part of $\rho(m, n)$. With hindsight this is apparent from examination of the stress-strain curves; they are almost not hysteretic. One of the virtues of the simulated annealing procedure is that it does not need to be prompted to find this structure. Rather, it has the freedom to find this or any other solution that is consistent with the data. A PM space density of the analytic form in (14) suggests two alternative methods for finding $\rho(m, n)$.

Normal Modes

The SA procedure uses the experimental modulus to constrain row and column sums in PM space. We postulate in (14) that each of these constraints is the sum of a diagonal and an off-diagonal contribution. It is possible to study the background and diagonal separately by considering the difference between two values of the strain at the same pressure (decreasing and increasing)

$$C_k = \epsilon(k)_\downarrow - \epsilon(k)_\uparrow = \sum_{m=k+1}^{N-1} \sum_{n=0}^k \rho_B(m, n). \quad (15)$$

The sum on the right-hand side is over the contents of a rectangular collection of bins that are part of the background only. There are $N - 1$ nontrivial strain differences at P_k , where $k = 0, \dots, N - 2$. These differences are $N - 1$ strain constraints on the background density. The normal mode method uses the strain constraints of (15) to find $\rho_B(m, n)$, $m \neq n$, in (14). Modulus constraints then determine the diagonal parts of ρ .

Let us suppose that we can describe the background density with a complete set of orthonormal functions that span PM space, $\phi_\alpha(m, n)$. We expand the density $\rho_B(m, n)$ in terms of these functions,

$$\rho_B(m, n) = \sum_{\alpha} b_{\alpha} \phi_{\alpha}(m, n). \quad (16)$$

Given (16), the strain constraints are a set of equations for the amplitudes b_{α} . As there are $N - 1$ strain constraints we can completely determine no more than $N - 1$ functions from the complete set. The inversion for the background density is again underdetermined. We impose an additional smoothness constraint like that in (13) and choose to use the longest wavelength modes from the complete set. The procedure is to minimize an energy, embodying the strain and smoothness constraints, by varying the $N - 1$ variational parameters b_{α} . Details of the procedure are discussed further in the appendix.

Exponential Decay

As most of the mechanical units are on the diagonal in PM space, it is plausible to assume that the density of mechanical units in the background of PM space decreases as one goes away from the diagonal. Let us adopt the analytic approximation

$$\rho_B(k, l) = \rho_B(k, k - 1)e^{-\kappa(k-1-l)}, \quad (17)$$

where $l = 0, \dots, k - 1$ and $k = 1, \dots, N - 1$.

The strain constraints on the background density given by (15) are constraints on the sum on $\rho_B(m, n)$ for a sequence of overlapping rectangles. The exponential decay procedure is to start with the smallest rectangle, at $m = N - 1$, $n = 0, \dots, N - 2$. We adopt the analytic approximation in (17) and take κ as known, e.g., $e^{-\kappa} = 0.9$. Then ρ_B in column $N - 1$ is given by

$$\rho_B(N - 1, n) = \rho_B(N - 1, N - 2)e^{-\kappa(N-2-n)}, \quad (18)$$

$$C_{N-2} = \rho_B(N - 1, N - 2) \sum_{n=0}^{N-2} e^{-\kappa(N-2-n)}, \quad (19)$$

or

$$\rho_B(N - 1, N - 2) = \frac{C_{N-2}}{\sum_{n=0}^{N-2} e^{-\kappa(N-2-n)}}. \quad (20)$$

Substituting $\rho_B(N - 1, N - 2)$ into (18), we know the content of the background bins in the column $N - 1$. The next constraint we look at involves bins in this column and bins in the column to the immediate left, $m = N - 2$. If we assume the same analytic form as

in (18) for column $N - 2$, we can find the amplitude that describes the bins in this column. We proceed in this manner going next to the constraint involving columns $N - 3$, $N - 2$, and $N - 1$. In this way we systematically develop the entire background density. Using the modulus constraints, we find the diagonal part of $\rho(m, n)$.

Results

In this section we describe the application of SA, NM, and ED to three data sets denoted B1, B2, and C. These are stress-strain data sets on sandstones.

1. B1 refers to a data set on Berea sandstone attributed to *Boitnott* [1993]. The B1 data set consists of a series of smaller and smaller stress-strain loops, shown in Figure 1; the pressure protocol is shown as an inset.

2. B2 refers to a data set on Berea sandstone attributed to *Hilbert et al.* [1994]. This data set consists of a single, large, closed stress-strain loop and eight small loops that are generated as the large loop is traversed. The data set and pressure protocol are shown in Figure 2.

3. C refers to a data set on Castlegate sandstone attributed to *Plona and Cook* [1995]. This data set consists of a series of large stress-strain loops and a sequence of small loops in the interior. The data set and pressure protocol are shown in Figure 3.

We will describe the analysis of these data sets as follows. First we use SA, NM, and ED on a single data set, B1, in order to characterize the three methods of inversion. Then we employ NM on all three data sets. We invert for the PM space density for each data set and use it to predict features in the stress-strain response and make a quantitative assessment of the linear and nonlinear elastic constants.

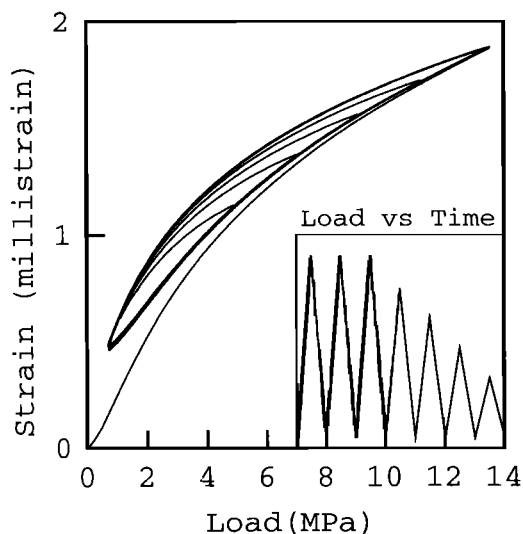


Figure 1. Experimental load versus strain for the Berea sandstone sample designated B1. Increasing pressure is the lower part of each strain loop. The pressure protocol is shown in the inset. The second pressure loop (1 MPa \rightarrow 14 MPa \rightarrow 1 MPa) was used to find the density in Preisach-Mayergoysz (PM) space [*Preisach*, 1935; *Mayergoysz*, 1985].

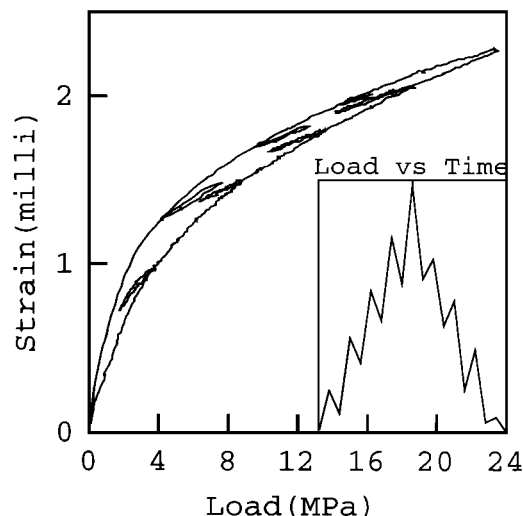


Figure 2. Experimental load versus strain for the Berea sandstone sample designated B2. Increasing pressure is the lower part of each strain loop. The pressure protocol is shown in the inset. The large pressure loop (0 MPa \rightarrow 24 MPa \rightarrow 0 MPa) was used to find the density in PM space.

Analysis of B1 data

We invert the second stress-strain loop in the B1 data set for $\rho(P_c, P_o)$ using SA, NM, and ED. From each PM space we predict the modulus as a function of pressure for the four smaller loops in Figure 1 and compare our results to experiment.

The data on the second loop span the pressure range (0.7186 MPa, 13.5502 MPa). The corresponding strain range is (0.0007, 0.0024). The pressure interval is broken into 30 bins using $\Delta P = 0.4277$ MPa. At each of

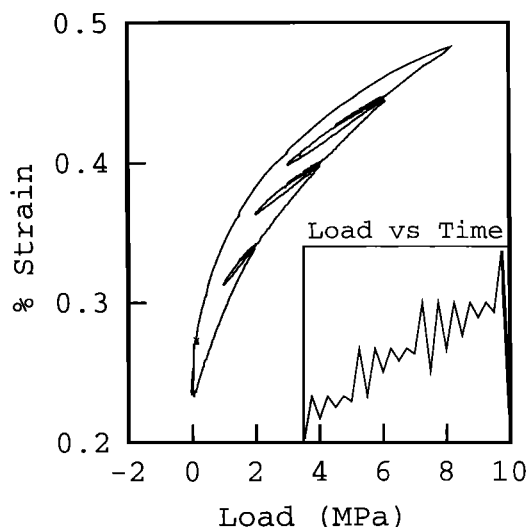


Figure 3. Experimental load versus strain for the Castlegate sandstone sample designated C. Increasing pressure is the lower part of each strain loop. The pressure protocol is shown in the inset. The small pressure loop (6 MPa \rightarrow 3 MPa \rightarrow 6 MPa) was used to find the density in PM space.

the pressures, $P_k = 0.7186 + k\Delta P$, where $k = 0, \dots, 29$, we find the value of the strain and the inverse modulus from the data. As a practical matter, our procedure for doing this is to fit the experimental strain data (the stress-strain curve for pressure increase and, separately, the stress-strain curve for pressure decrease) to a 10-term polynomial in P , obtaining $Q_{10}^\uparrow(P)$ and $Q_{10}^\downarrow(P)$, respectively. We evaluate these polynomials at P_k to obtain the values of the strain at pressure P_k . To find the inverse modulus on pressure increase (decrease), we take the derivative of the polynomial Q_{10}^\uparrow (Q_{10}^\downarrow) analytically and evaluate it at P_k .

Simulated annealing method on B1. The 30 values of $K_\uparrow(k)$ are 30 constraints on the column sums in PM space; the 30 values of $K_\downarrow(k)$ are 30 constraints on the row sums in PM space. The sum of the column constraints is equal to the sum of the row constraints, and both are equal to the total number of mechanical units in PM space. As the physical quantities are proportional to the fraction of mechanical elements in PM space, we take the total number of mechanical units to be a convenient number, in this case, 5000. To the modulus constraints we add four smoothness constraints. These are near neighbors in the x and y direction, i.e., $[\rho(m+1, n) - \rho(m, n)]^2$ and $[\rho(m, n+1) - \rho(m, n)]^2$, and next near neighbors, parallel and perpendicular to the diagonal, i.e., $[\rho(m+1, n+1) - \rho(m, n)]^2$ and $[\rho(m, n) - \rho(m+1, n-1)]^2$. The smoothness parameter $\lambda = 3$. The annealing procedure is started at high tem-

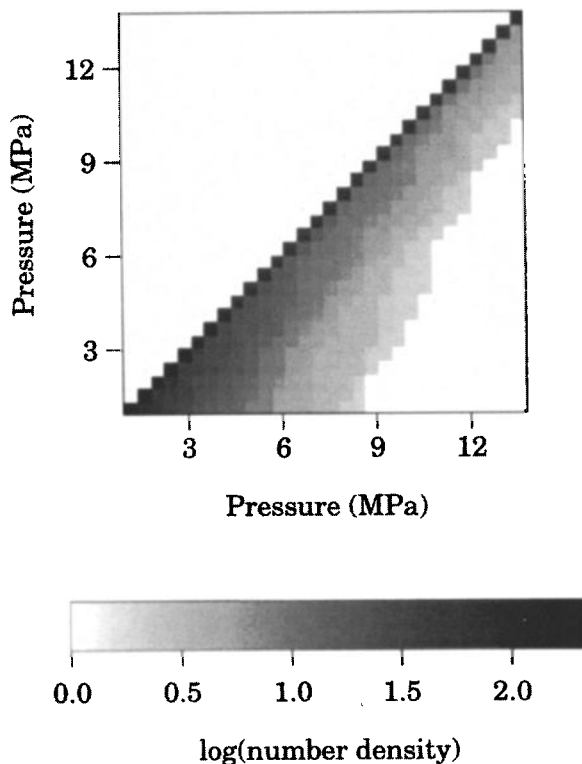


Figure 4. B1 PM space density using simulated annealing (SA) method. The density $\rho(m, n)$ for the B1 sample, found using the SA method, is shown as a function of (m, n) using a logarithmic gray scale.

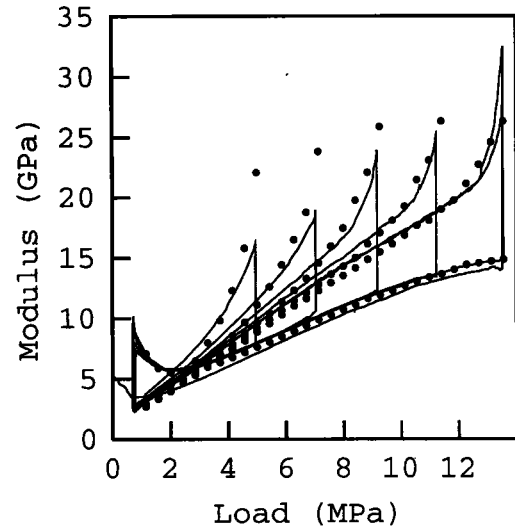


Figure 5. B1 modulus versus pressure from SA results. The modulus is plotted as a function of the load for sample B1. Increasing pressure is the lower part of each modulus loop. The solid line is the experimental data; the solid circles are the predicted modulus using the PM space density determined by the method of simulated annealing.

perature, and the temperature is reduced by a factor of 0.9 at each iteration. An iteration consists of 5×10^4 unit moves or 5×10^5 tries [Press et al., 1992]. Convergence occurs in 80–150 iterations. An SA inversion of this size requires 15–25 min of computer time on an HP715/100 workstation.

The results of using the SA method are shown in Figure 4, a gray scale plot of the PM space density using the logarithmic gray scale below the figure. The hysteretic mechanical elements, those off the diagonal, have density much lower than the nonhysteretic elements, those on the diagonal. The background density falls off as one moves away from the diagonal.

The modulus as a function of pressure for various pressure protocols can be calculated from PM space using (8b) and (9b). We use $\rho(P_c, P_o)$ to calculate the modulus as a function of pressure for the four pressure loops in the latter part of the B1 pressure protocol. The experimental modulus versus pressure and the predicted modulus versus pressure are shown in Figure 5. Since the agreement between the two sets of curves is quite good, we conclude that the SA analysis of a single large loop gives us predictive capability for smaller loops.

Normal mode method on B1. The 29 values of the strain differences at pressures P_k , $k = 0, \dots, N-2$, are strain constraints on the background. We use the 29 lowest modes of the complete set $\phi_{\mu\nu}(m, n)$ with $(\mu, \nu) = (0, 0), (1, 0), \dots, (5, 5), (6, 4), (7, 2)$, as defined in the appendix. The smoothing involves springs in the x and y directions, leading to an energy that penalizes short-wavelength modes. For the strength of the quadratic smoothing we use $\lambda = 0.2$. The calculation requires the inversion of a 29×29 matrix, a matter of seconds on a workstation.

The results of the NM inversion for the B1 data set are shown in Figure 6; $\rho(m, n)$ in arbitrary units is plotted as a function of (m, n) . To facilitate comparison of Figure 6 with Figure 4, we have used 5000 mechanical units and the same gray scale in both figures. The NM PM space density is qualitatively and quantitatively similar (but not identical) to the SA PM space density.

Using the PM space density shown in Figure 6, (8a), and (9a), we find the modulus versus pressure curves appropriate to the last four loops in the experimental pressure protocol. The predicted modulus is shown in Figure 7 along with the corresponding experimental data curves. As with the simulated annealing case, the agreement between prediction and experiment is quite good.

Exponential decay method on B1. The 29 values of the strain difference at the 29 pressures $P_k = 0.7186 + k\Delta P$, $k = 0, \dots, 28$ are 29 constraints on the background. We chose $\kappa \approx 0.1$, $e^{-\kappa} = 0.90$, in (17) for our calculations. The calculation takes negligible computer time. The exponential decay method leads to the PM space density shown in Figure 8. As with the other two methods, the total number of mechanical units has been taken to be 5000 to facilitate direct comparison of the PM space densities. Use of this PM space density, (8a), and (9a) leads to the modulus pressure curves shown in Figure 9.

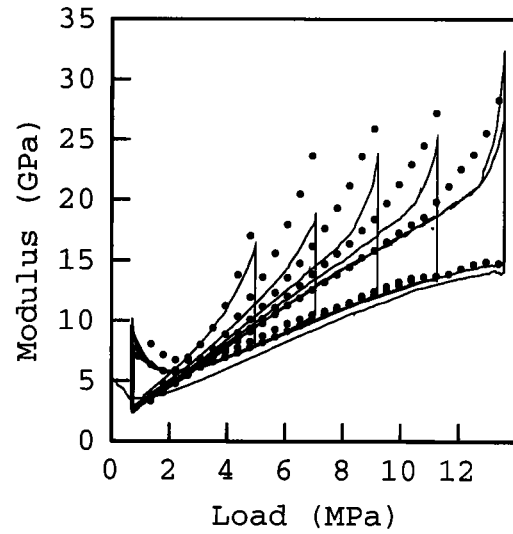


Figure 7. B1 modulus versus pressure from NM results. The modulus is plotted as a function of the load for sample B1. Increasing pressure is the lower part of each modulus loop. The solid line is the experimental data; the solid circles are the predicted modulus using the PM space density determined by the method of normal modes.

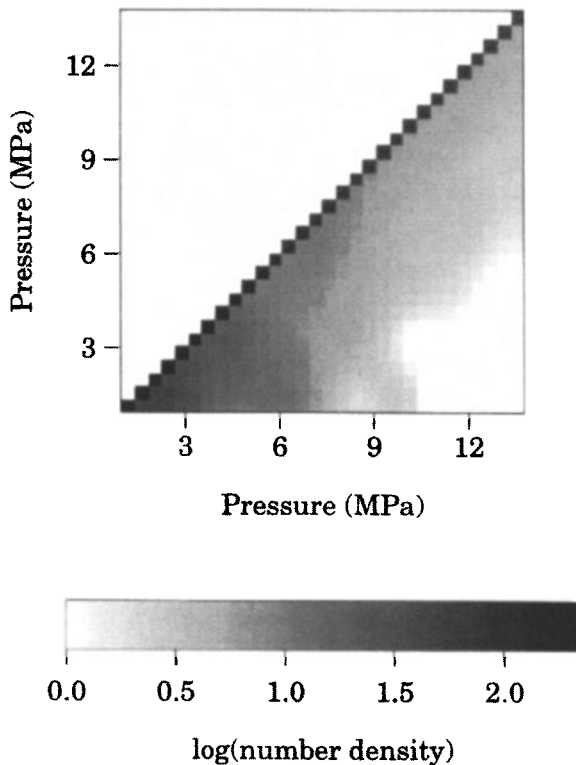


Figure 6. B1 PM space density using normal modes (NM) method. The density $\rho(m, n)$ for the B1 sample, found using the NA method, is shown as a function of (m, n) using a logarithmic gray scale.

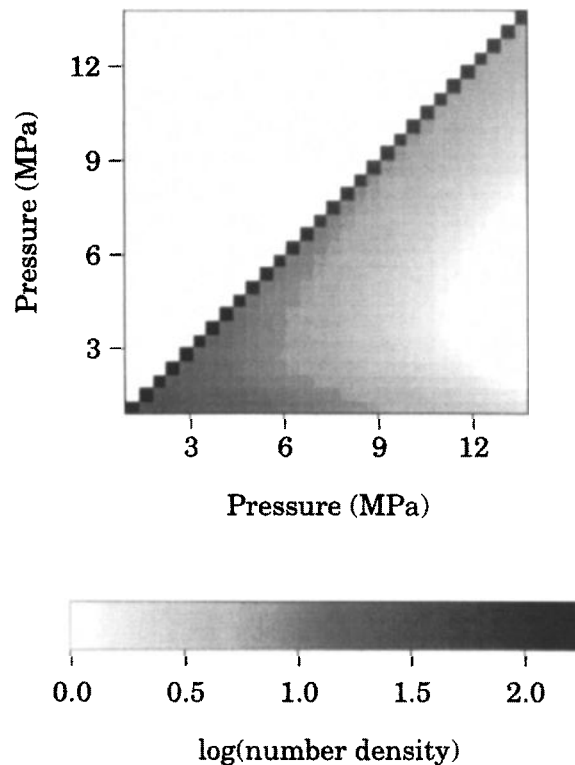


Figure 8. B1 PM space density using exponential decay (ED) method. The density $\rho(m, n)$ for the B1 sample, found using the ED method, is shown as a function of (m, n) using a logarithmic gray scale.

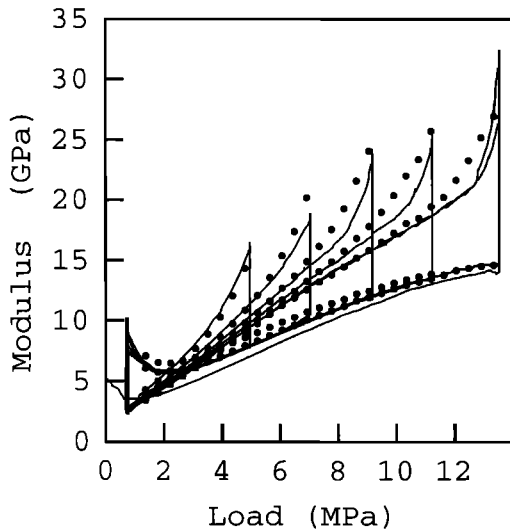


Figure 9. B1 modulus versus pressure from ED results. The modulus is plotted as a function of the load for sample B1. Increasing pressure is the lower part of each modulus loop. The solid line is the experimental data; the solid circles are the predicted modulus using the PM space density determined by the method of exponential decay.

Comparison of the three methods of inversion.

Figures 5, 7, and 9 show the modulus-pressure curves found from three different solutions to the problem of inverting stress-strain data for the PM space density. In each case the modulus pressure curves are in good agreement with experiment. Each method has particular positive and negative features.

The SA method is the least biased by our assumptions about the structure of PM space. The SA filling of PM space is flexible because there are as many variational parameters as there are bins. However, the SA method requires an order of magnitude more computational time than the NM method.

The NM method reduces the number of variational parameters by an order of magnitude over the SA method but does not a priori enforce a particular density distribution. The NM method is very fast, requiring only the inversion of an $N \times N$ matrix. However, the choice of normal modes will influence the superficial structure of PM space. For example, our choice of cosines as normal modes produces a small sinusoidal variation in the PM space structure. This is most pronounced in the analysis of the Castlegate sandstone data.

The ED method is the most biased by our assumptions. It is the fastest computationally because the ED method leaves only one parameter to be chosen by the operator. The ED method enforces a PM space that is exponentially decaying away from the diagonal. Thus we may inadvertently miss interesting structure in the PM space of unusual rock samples.

Our results do not constrain our choice of method. We prefer the NM method. It is a compromise between the SA method, having as many variational param-

eters as there are bins, and the ED method, having one parameter and a definite prejudice as to the behavior of the density. In addition, the NM method requires less computer time than the SA method, although it requires more computer time than the ED method. Below, we illustrate the use of the NM method on all three data sets.

Normal Mode Method on B1, B2, and C

B1. The previous section contains the PM space density for the B1 sample using the NM method of analysis (Figure 6). Figure 7 shows the result of using this PM space density to predict the elastic response to pressure protocols other than the one used in finding the density. It is possible to study other elastic properties using the PM space density. From (10b) and prior discussion we see that the dynamic modulus is determined by the diagonal part of the PM space density. As a practical recipe, we have

$$\frac{1}{K_d(k)} = \Delta \epsilon \rho(k, k) \Delta P. \quad (21)$$

where K_d is the dynamic modulus and $\rho(k, k)$ is the fraction of the mechanical units on the diagonal at P_k . The dynamic elastic modulus calculated by this procedure is shown in Figure 10. Also shown on the figure are the static elastic moduli calculated from the experimental data. There are two static curves, one for pressure increase and one for pressure decrease.

The dynamic modulus in Figure 10 is an increasing function of the pressure with a long-wavelength sinu-

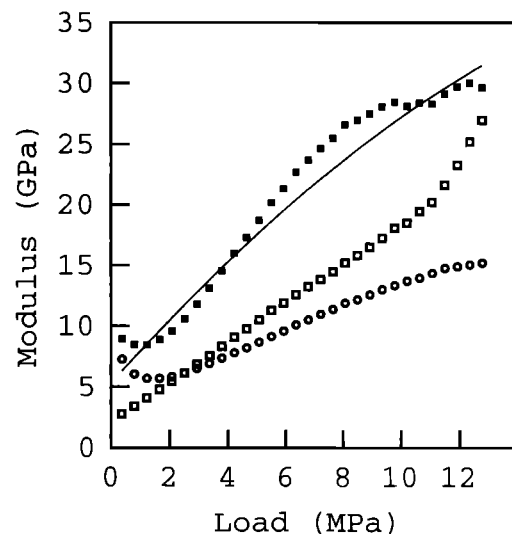


Figure 10. B1 moduli versus pressure from NM results. The open circles are the static data for pressure increase from the experimental data, i.e., from the second pressure loop described in Figure 1. The open squares are the static modulus for pressure decrease. The solid squares are the dynamic modulus calculated from the diagonal component of the PM space density. The solid line is the quadratic fit to the dynamic modulus.

soidal deviation from the smooth curve described below. The dynamic modulus result comes from a single cell in PM space rather than an average over many cells. Thus the estimated error bars are approximately the height of the sinusoidal deviation. The dynamic modulus is at every pressure greater than the static modulus. The two moduli would be equal only if there were no off-diagonal mechanical elements. The dynamic modulus and the static modulus are almost equal at the points of pressure reversal in the pressure protocol. This is in agreement with theory [McCall and Guyer, 1994].

The dynamic modulus found from the density in PM space can be used to estimate the nonlinear elastic constants. We define the dynamic modulus as a function of the strain field

$$K_d = \bar{K} [1 + \beta \nabla \cdot \mathbf{u} + \delta (\nabla \cdot \mathbf{u})^2] \quad (22)$$

where β and δ are the nonlinear elastic coefficients, dimensionless measures of the cubic and quartic anharmonicities, and \mathbf{u} is the displacement. Since K_d is minus the derivative of P with respect to the strain we use

$$\frac{P}{\bar{K}} = -\nabla \cdot \mathbf{u} - \frac{\beta}{2} (\nabla \cdot \mathbf{u})^2 - \frac{\delta}{3} (\nabla \cdot \mathbf{u})^3 \quad (23)$$

to write K_d as a power series in P .

$$K_d = \bar{K} \left[1 + a \frac{P}{\bar{K}} + b \left(\frac{P}{\bar{K}} \right)^2 \right] \quad (24)$$

where

$$a = -\beta \quad (25)$$

$$b\bar{K} = \delta - \frac{\beta^2}{2}. \quad (26)$$

To find a and b , we fit the dynamic modulus shown in Figure 10 to (24) with the pressure variable P replaced by $P - \bar{P}$. Here \bar{P} is the average pressure and \bar{K} is the average modulus. Thus the β and δ that we find characterize the entire dynamic modulus curve. The smooth curve determined in this way is shown in Figure 10. We find $\bar{P} = 7.22$ MPa and $\bar{K} = 23.28$ GPa. In Table 1 we list the values of β and δ found from this analysis. Note the magnitude of the cubic anharmonicity is approximately 10^3 , about 2 orders of magnitude greater than for normal materials. In general, consolidated materials are very anharmonic compared to normal mate-

Table 1. Predicted Dynamic Modulus β and δ From Normal Mode Preisach-Mayergoyz Space

Sample	\bar{P} , MPa	\bar{K} , GPa	β	$\delta \times 10^{-6}$
B1	7.22	23.28	-1805	-1.76
B2	11.93	29.16	-1661	-0.66

\bar{P} is average pressure, and \bar{K} is average modulus. Calculations are based on the average pressure over the range of the experimental data and (24)–(26).

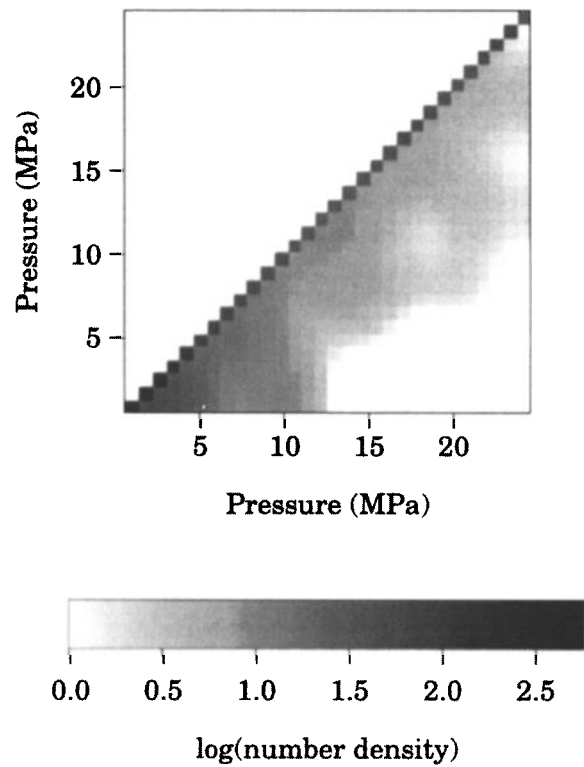


Figure 11. B2 PM space density using NM. The density $\rho(m, n)$ for the B2 sample, found using the method of normal modes, is shown as a function of (m, n) using a logarithmic gray scale.

rials. The quartic anharmonicity δ is of the order of magnitude of β^2 . This is characteristic of consolidated materials; the most striking changes in modulus occur below pressures of order \bar{K} .

B2. We used the large stress-strain pressure loop shown in Figure 2 to invert for the B2 PM space density using the method of normal modes. The resulting PM space density is shown in Figure 11 on a logarithmic gray scale. The PM space density shown on Figure 11 was used to predict the eight small loops in the experiment on sample B2. The results are shown in Figure 12. The inset of this figure is the fourth small loop on pressure increase.

From the PM space density we can calculate the dynamic modulus using (10b). The result is shown in Figure 13, where we also show the two static moduli calculated from the experimental data. As we found for sample B1, the dynamic modulus is greater than the static modulus at all pressures. The oscillation of the dynamic modulus is evidence of the normal mode method we have employed, and we find that the error bars are of order the oscillation.

As we did for sample B1, we can use a smooth curve through the dynamic modulus to determine the strength of the anharmonicities. We find $\bar{P} = 11.93$ MPa and $\bar{K} = 29.16$ GPa. The values of β and δ derived from this procedure are listed in Table 1. We note that β is about the same for both Berea samples. The coefficient $b\bar{K}$ (see (24)) is quite close for the two sam-

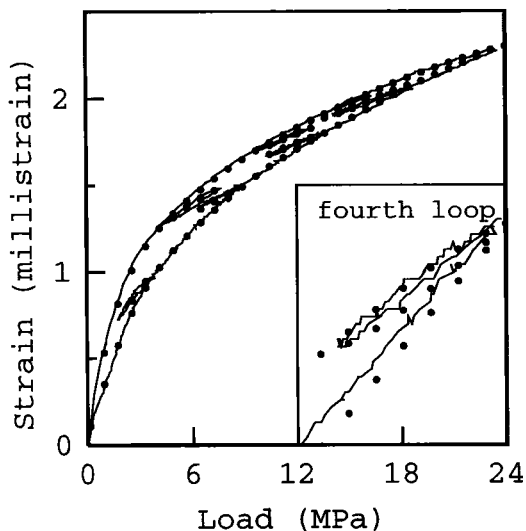


Figure 12. Comparison of strain versus load from data and the NM prediction for the B2 sample. The solid line is the experimental data; the solid circles are the prediction from PM space. The inset shows an expanded view of the fourth loop on pressure increase.

ples (B1, $b\bar{K} = -1.8 \times 10^6$, B2, $b\bar{K} = -1.24 \times 10^6$); however, the combination of $b\bar{K}$ and β yielding δ for sample B2 is smaller than for B1.

C. For the C sample we looked at the five small loops that start at about 6 MPa (see the pressure protocol inset in Figure 3). These loops are shown in Figure 14, separated so that they can be seen easily. We used the largest of these loops to determine the PM space density for mechanical units in the range 3–6 MPa. This pressure range is modest so we used only 10 bins in PM space, $\Delta P \approx 0.3$ MPa. The PM space

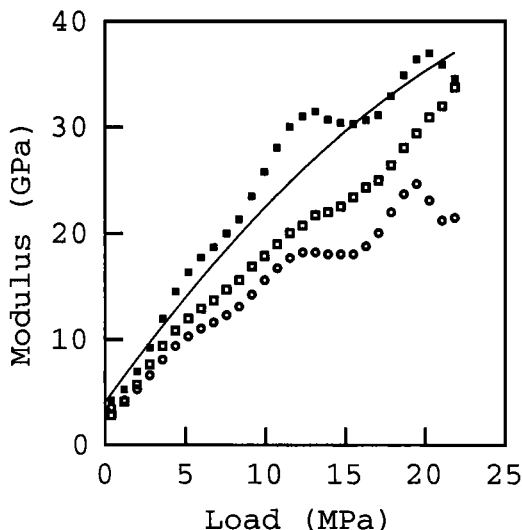


Figure 13. B2 moduli versus pressure from NM results. The open circles are the static modulus for pressure increase from the experimental data. The open squares are the static modulus for pressure decrease. The solid squares are the dynamic modulus calculated from the diagonal component of the PM space density. The solid line is the quadratic fit to the dynamic modulus curve.

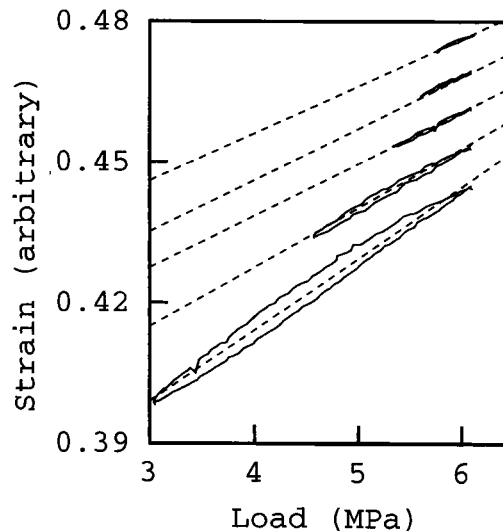


Figure 14. C stress-strain data. In Figure 3 there are five pressure loops that begin at $P \approx 6$ MPa. These five loops are shown here with a vertical shift between loops. The line through each loop is a linear fit to all of the data points in the loop. The slopes of the linear fits are plotted in Figure 17 as solid squares. A PM space density was determined for sample C using the largest of these loops.

density that we found using the NM method is shown in Figure 15. In this figure the sinusoidal character of our choice of normal modes is evident in the spurious minimum close to the diagonal at $P \approx 5$ MPa.

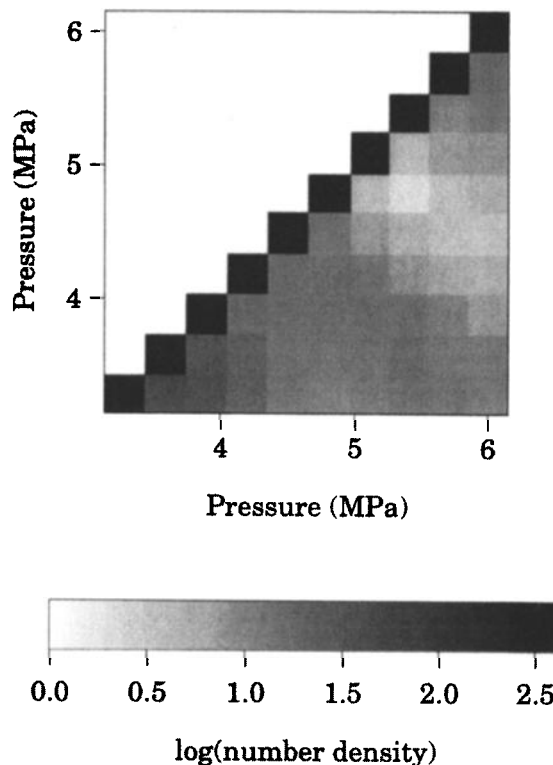


Figure 15. C PM space density using NM. The density $\rho(m, n)$ for the C sample, found using the method of normal modes, is shown as a function of (m, n) using a logarithmic gray scale.

The PM space density shown in Figure 15 was used to predict the behavior of the four smaller loops. These predictions are shown in Figure 16, shifted above the experimental data for clarity. On this figure we show a second set of predicted stress-strain loops, generated by a pressure protocol that begins at $P = 3$ MPa, advances to $P = 4.5$ MPa, and then makes a sequence of seven smaller and smaller downward loops from $P = 4.5$ MPa. From the stress-strain curves in Figure 16 we found a variety of moduli, plotted in Figure 17.

1. The static modulus of the large experimental loop for pressure increase is shown as the open circles in Figure 17.

2. The average modulus of the five experimental loops in Figure 14 is shown as the solid squares in Figure 17. For the average modulus of a loop we take the slope of a line, $y = mx + b$, fit to all of the data points on the loop. The average modulus is assigned to the pressure that is the average of the pressure range spanned by the loop. Thus the largest downward loop from $P = 6$ MPa has the lowest average pressure and is the most leftward of the five solid squares in Figure 17.

3. The average modulus for the sequence of seven loops, predicted using the PM space density, that begin and end at $P = 4.5$ MPa is shown as the solid circles in Figure 17.

4. The dynamic modulus calculated from the PM space density shown in Figure 15 is shown as the open squares on Figure 17.

5. The dynamic modulus calculated from experimental measurement of the longitudinal and transverse sound velocity in sample C [Plona and Cook, 1995] is shown as the crosses in Figure 17. These measurements

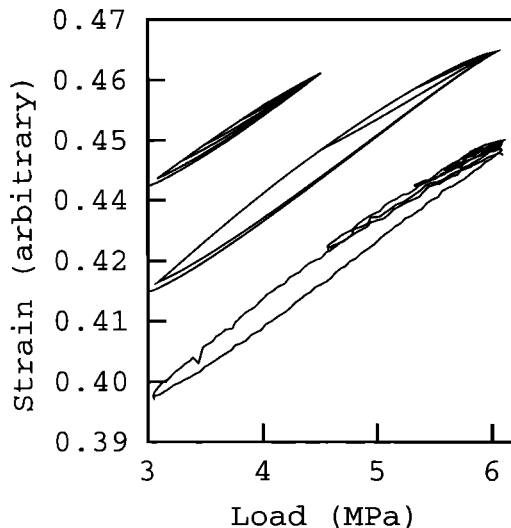


Figure 16. Comparison of strain versus load from data and the NM prediction for the C sample. The bottom set of loops is the data in Figure 14; the middle set of loops (displaced for clarity) is the prediction for the behavior of the four smaller loops from the PM space for the largest loop. The top set of loops is a sequence of stress-strain loops predicted for a pressure protocol beginning at 4.5 MPa. The average slope of these loops is plotted in Figure 17 as solid circles.

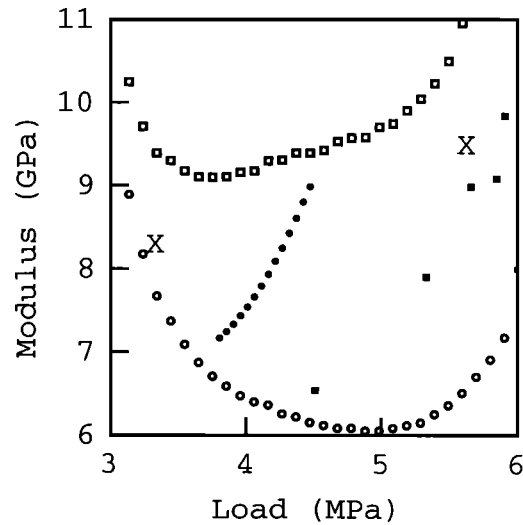


Figure 17. C moduli versus pressure from NM results. The open circles are the static modulus on pressure increase from the data on the largest loop. The open squares are the dynamic modulus calculated from the diagonal part of the PM space density. The solid squares are the sequence of slopes of the experimental loops shown in Figure 14 and plotted at the average pressure of the loop. The solid circles are the sequence of slopes of the predicted loops terminating at 4.5 MPa in Figure 16. The crosses are the dynamic modulus determined from direct measurement of the longitudinal and transverse velocities of sound.

were made simultaneously with the stress-strain measurement.

A number of observations can be made about the five moduli shown on Figure 17. (1) The dynamic modulus calculated from the PM space density is greater than the static moduli at every pressure. (2) A sequence of average moduli evolves from approximately the static modulus to approximately the dynamic modulus as the size of the loop decreases. (3) The dynamic modulus found from the PM space density is in good agreement with the measured value of the dynamic modulus.

Conclusions

In this paper we have introduced three methods for solution of the PM space inverse problem (simulated annealing, normal modes, and exponential decay) and tested them using three stress-strain data sets on sandstones (B1, B2, and C). We applied all three methods to the B1 data set. From the data set we found the PM space density ρ and used it to predict the behavior of a sequence of quasi-static stress-strain curves. The resulting three sets of quasi-static stress-strain curves did not provide the means to make a definitive choice among methods. Considering flexibility (the ability to give an unanticipated result) and computation time, we feel that the method of normal modes is most valuable. We used this method to look further at the B1 data set and at the B2 and C data sets. We find the following.

1. The PM space density is well described by a diagonal plus background structure, as in (14). Almost 50%

of the mechanical elements are in the background; that is, almost 50% of the mechanical elements in a rock are hysteretic.

2. The three data sets cover different pressure ranges: 3 MPa, 12 MPa, and 24 MPa for the C, B1, and B2 data sets, respectively. The PM space density is most uniform for sample C, the smallest pressure range, and least uniform for sample B2, the largest pressure range. As the variation in pressure and strain increases, the inverse problem becomes more difficult to constrain.

3. PM space for samples B1 and B2 contains the highest density of hysteretic mechanical units at low pressure. This implies that the hysteretic behavior of rocks is due to mechanical units with maximum compliance at low pressure. At high pressure the rock tends to the elastic properties of the grain material with greatly reduced hysteresis. It is this qualitative property that gives both the sign and order of magnitude of β and δ .

4. The signs and orders of magnitude of the nonlinear coefficients β and δ are in agreement with prior estimates [Winkler and Xingzhou, 1996]. However, reliable estimates of dynamic elastic characteristics from static elastic properties requires further theoretical and experimental development. For example, better estimates of nonlinear coefficients require more accurate assignments of the diagonal density $\rho(k, k)$. We may want to reduce the bin size in PM space to get a better dynamic estimate; however, the inversion problem is then less constrained. One way to add constraints is to use more data. A small stress-strain loop defines a small part of PM space; a larger stress-strain loop constrains a PM space that is already partly defined by the small loop.

5. The theoretical model we have employed connects the behavior of the individual mechanical elements to the elastic properties of a statistical ensemble in the simplest possible manner, e.g., mechanical elements enforcing one of two lengths. When more complex mechanical elements are considered, e.g., soft and stiff spring constants, the relationship between the strain and the density in PM space remains qualitatively the same, although the analytic derivation of the PM space-strain relationship is more complex.

6. Rocks have elastic properties similar to those of other consolidated materials (e.g., soils, cements, ceramics), and the ideas behind our treatment of rocks have the potential to be useful beyond geophysics.

Appendix: Normal Modes Procedure

PM space is covered by bins (m, n) , where $m = 0, \dots, N-1$, and $n = 0, \dots, N-1$ and $N\Delta P$ is the maximum pressure. The background portion of PM space $\rho_B(m, n)$ is the set of bins forming the triangle with corners $(1, 0)$, $(N-1, 0)$, and $(N-1, N-2)$. There are $N-1$ constraints on the background density; thus we can constrain at most $N-1$ normal modes in (16).

Symmetry can be used to advantage in the normal mode calculation, thus we define a function $\eta(i, j)$ such that for $i, j = 0, \dots, N-2$, $\eta(i, j) = \rho_B(i+1, j)$. We define η over the range $-(N-2) \leq i, j \leq N-2$,

and impose an eightfold symmetry such that $\eta(i, j) = \eta(-i, j) = \eta(i, -j) = \eta(-i, -j) = \eta(j, i) = \eta(j, -i) = \eta(-j, i) = \eta(-j, -i)$. The function η is periodic over $2N-4$, i.e., $\eta(i+2N-4, j) = \eta(i, j+2N-4) = \eta(i, j)$. To describe η in terms of normal modes, we use the set of functions

$$\begin{aligned} \phi_\alpha(i, j) &= \phi_{\mu\nu}(i, j) \\ &= \frac{1}{\sqrt{2}(N-2)} \left[\cos\left(\frac{\pi\mu i}{N-2}\right) \cos\left(\frac{\pi\nu j}{N-2}\right) \right. \\ &\quad \left. + \cos\left(\frac{\pi\nu i}{N-2}\right) \cos\left(\frac{\pi\mu j}{N-2}\right) \right], \end{aligned} \quad (\text{A1})$$

where α , μ , and ν are positive integers.

Write $\eta(i, j)$ as a sum over $N-1$ normal modes,

$$\eta(i, j) = \sum_{\alpha=0}^{N-2} b_\alpha \phi_\alpha(i, j), \quad (\text{A2})$$

where the amplitudes b_α are to be determined. The experimental strain constraints given by (15) are incorporated into an energy,

$$E_C = \frac{1}{2} \sum_{k=0}^{N-2} \left[C_k - \sum_{\alpha=0}^{N-2} a_{k\alpha} b_\alpha \right]^2, \quad (\text{A3})$$

where

$$a_{k\alpha} = \sum_{i=k}^{N-2} \sum_{j=0}^k \phi_\alpha(i, j). \quad (\text{A4})$$

The background density is smoothed by an energy smoothing η ,

$$\begin{aligned} E_S &= \frac{1}{2} \sum_{i,j=-N+3}^{N-2} \left\{ [\eta(i+1, j) - \eta(i, j)]^2 \right. \\ &\quad \left. + [\eta(i, j+1) - \eta(i, j)]^2 \right\}. \end{aligned} \quad (\text{A5})$$

By symmetry, $\eta(N-1, j) = \eta(-N+3, j)$ and $\eta(i, N-1) = \eta(i, -N+3)$. Using the normalization properties of sums of cosines and sines, we have

$$E_S = \sum_{\mu=0}^{\mu_{\max}} \sum_{\nu=0}^{\nu_{\max}} S_{\mu\nu} b_{\mu\nu}^2, \quad (\text{A6})$$

where

$$S_{\mu\nu} = 4 \left(\sin^2 \frac{\pi\mu}{2N-4} + \sin^2 \frac{\pi\nu}{2N-4} \right), \quad (\text{A7})$$

μ_{\max} and ν_{\max} are chosen such that the total number of states is $N-1$, and $\nu \leq \mu$ for any particular state.

The equations for the amplitudes are found by varying the total energy $E_C + \lambda E_S$ with respect to b_γ , where γ is a particular choice of the coefficients. The parameter λ determines the relative importance of smoothing as compared to satisfying the constraints. The resulting equation is

$$\sum_{\alpha=0}^{N-2} (A_{\alpha\gamma} - \lambda S_{\gamma} \delta_{\alpha,\gamma}) b_{\alpha} = B_{\gamma}, \quad (\text{A8})$$

where

$$A_{\alpha\gamma} = \sum_{k=0}^{N-2} a_{k\alpha} a_{k\gamma}, \quad (\text{A9})$$

$$B_{\gamma} = \sum_{k=0}^{N-2} C_k a_{k\gamma}. \quad (\text{A10})$$

The procedure is to choose λ , construct a , A , and B , and solve the linear system in (A8) for the set of b_{α} .

Acknowledgments. We thank P. A. Johnson, A. Kadish, T. J. Shankland, J. A. TenCate, and K. E. A. Van Den Abele for continued interest and helpful discussions. This work has partial support from OBES, Engineering and Geosciences grant W7405-ENG-36, the National Science Foundation grant EAR-9528965, and the Institute of Geophysics and Planetary Physics at Los Alamos National Laboratory.

References

- Ashcroft, N. W., and N. D. Mermin, *Solid State Physics*, Holt, Rinehart, and Winston, Austin, Tex., 1976.
- Biot, M. A., Thermoelasticity and irreversible thermodynamics, *J. Appl. Phys.*, **27**, 240, 1956.
- Boitnott, G. N., Fundamental observations concerning hysteresis in the deformation of intact and jointed rock with applications to nonlinear attenuation in the near source region, in *Proceedings of the Numerical Modeling for Underground Nuclear Test Monitoring Symposium, Los Alamos Natl. Lab. Rep., LA-UR-93-3839*, 121, 1993.
- Guyer, R. A., K. R. McCall, and G. N. Boitnott, Hysteresis, discrete memory, and nonlinear wave propagation in rock: A new paradigm, *Phys. Rev. Lett.*, **74**, 3491, 1995.
- Hamilton, M. F., Fundamentals and applications of nonlinear acoustics, in *Nonlinear Wave Propagation in Mechanics*, edited by T. W. Wright, p. 1, Am. Soc. of Mech. Eng., New York, 1986.
- Hilbert, L. B., Jr., T. K. Hwong, N. G. W. Cook, K. T. Nihei, and L. R. Myer, Effects of strain amplitude on the static and dynamic nonlinear deformation of Berea sandstone, in *Rock Mechanics Models and Measurements Challenges from Industry*, edited by P. P. Nelson and S. E. Laubach, p. 497, A. A. Balkema, Rotterdam, Netherlands, 1994.
- Holcomb, D. J., Memory, relaxation, and microfracturing in dilatant rock, *J. Geophys. Res.*, **86**, 6235, 1981.
- Landau, L. D., and E. M. Lifshitz, *Theory of Elasticity*, Pergamon, Tarrytown, N. Y., 1959.
- Mayergoyz, J. D., Hysteresis models from the mathematical and control theory points of view, *J. Appl. Phys.*, **57**, 3803, 1985.
- McCall, K. R., and R. A. Guyer, Equation of state and wave propagation in hysteretic nonlinear elastic materials, *J. Geophys. Res.*, **99**, 23,887, 1994.
- Metropolis, N., A. W. Rosenbluth, M. N. Rosenbluth, A. H. Teller, and E. Teller, Equation of state calculations by fast computing machines, *J. Chem. Phys.*, **21**, 1087, 1953.
- Murnaghan, F. D., *Finite Deformation of an Elastic Solid*, John Wiley, New York, 1951.
- Plona, T. J., and J. M. Cook, Effects of stress cycles on static and dynamic Young's moduli in Castlegate sandstone, in *Rock Mechanics: Proceedings of the 35th U.S. Symposium*, edited by J. J. K. Daemen and R. A. Schultz, p. 155, A. A. Balkema, Rotterdam, Netherlands, 1995.
- Preisach, F., Über die magnetische Nachwirkung, *Z. Phys.*, **94**, 277, 1935.
- Press, W. H., S. A. Teukolsky, W. T. Vetterling, and B. P. Flannery, *Numerical Recipes in FORTRAN, The Art of Scientific Computing*, Cambridge Univ. Press, New York, 1992.
- Winkler, K. W., and L. Xingzhou, Measurements of third-order elastic constants in rocks, *J. Acoust. Soc. Am.*, **100**, 1392, 1996.
- G. N. Boitnott, New England Research Inc., 76 Olcott Drive, White River Junction, VT 05001. (e-mail: boitnott@fly.ner.com)
- R. A. Guyer, Department of Physics and Astronomy, University of Massachusetts, Amherst, MA 01003. (e-mail: rag@cmp.phast.umass.edu)
- L. B. Hilbert Jr., Failure Analysis Associates, 149 Commonwealth Drive, Menlo Park, CA 94025. (e-mail: bhilbert@fail.com)
- K. R. McCall, Department of Physics, University of Nevada, Reno, NV 89557. (e-mail: mccall@physics.unr.edu)
- T. J. Plona, Schlumberger-Doll Research, Old Quarry Road, Ridgefield, CT 06877. (e-mail: plona@ridgefield.sdr.slb.com)

(Received May 16, 1996; revised October 25, 1996; accepted November 26, 1996.)